Heterodyne and Nonergodic Approach to Dynamic Light Scattering of Polymer Gels: Aqueous Xanthan in the Presence of Metal Ions (Aluminum(III))

Andrew B. Rodd,[†] Dave E. Dunstan,[†] David V. Boger,*[,†] Juergen Schmidt,[‡] and Walther Burchard[‡]

Department of Chemical Engineering, University of Melbourne, Melbourne, Australia; and Institute for Macromolecular Chemistry, University of Freiburg, 79104 Freiburg, Germany

Received October 2, 2000; Revised Manuscript Received February 2, 2001

ABSTRACT: Solutions of xanthan gum form a strong gel in the presence of metal ions. The gelation process of a low concentration xanthan solution in the presence of aqueous aluminum ions (Al(III)) was followed as a function of temperature. Thermal gelation was observed at 44 ± 2 °C by the onset of heterodyne and nonergodic behavior and by the divergence of the observed fast motion. The paper deals extensively with the main problem of light scattering from systems where long relaxation processes are occurring and the time average no longer coincides with the ensemble average. The two approaches suggested in the literature, i.e., the *heterodyne* and the *nonergodic* approach, developed by Geissler and Pusey, respectively, are tested. Two modes of motion are observed in the solution state as well as in the gel. The fast motions can be assigned to the collective diffusion of the gel modes. The relaxation time passes through a sharp maximum at the gel point and then decreases. The slow motions arise from clusters or heterogeneities. In the gel state the collective diffusion is superimposed by marked internal network fluctuations.

Introduction

Solutions of xanthan gum are well-known to gel in the presence of trivalent metal ions[1] via the formation of a dimeric or polymeric ionic bridge.[2] In particular, in the presence of aluminum ions, xanthan solutions form a semireversible gel that sets with the addition of heat.[3] This paper will examine the gelation of xanthan solutions in the presence of aluminum ions (Al(III)) by dynamic and static light scattering (DLS and SLS). It is the observed gelation upon the addition of heat that makes the xanthan−Al(III) system an ideal medium for testing two theoretical approaches[4,5] to the interpretation of time correlation functions obtained by dynamic light scattering.

The possibilities and problems arising in dynamic light scattering from gels has extensively been discussed by Geissler in a recent review article.[5] The majority of earlier papers concentrated on determining the longitudinal modulus and comparison to the elastic shear modulus.[6] Furthermore, the theoretical derivation by Tanaka et al.[7] led to the prediction of a collective diffusion coefficient D_C suggesting a certain concentration dependence that resembles the mutual diffusion coefficient in semidilute solutions should be observed.[5,8,9] This point, appears to be well understood and will not be addressed in this paper. Geissler[5] pointed out at the end of his article that the evaluation of data from apparently homogeneous gels, that appear fully transparent, may involve serious errors because of the heterodyne scattering, resulting from large inhomogeneity or, even worse, because of a "frozen-in" structure that causes typical nonergodic behavior. Nonergodic, in this context, suggests that the time average of the scattering intensity at one fixed sample orientation differs from the sample average, obtained from different orientations of the scattering cell. Geissler[5] suggested that the correct evaluation is still not satisfactorily solved. This intriguing problem has been addressed by a few other articles.[10−18] Among these, the important theoretical consideration of Panyukov and Rabin[14] will be discussed in detail in the context of our results. This paper was reviewed 2 years later by Shibayama[18] who, in addition to the static scattering profiles, considered the dynamic properties, where an even higher complexity was introduced.

The goal of our paper is to test the two approaches of heterodyne and nonergodic behavior with another gelling system to those that have been previously studied. The xanthan−Al(III) system forms a gel at very low polymer concentrations (as low as 0.1 mg/mL, i.e., 0.01% (w/v)). Such gels are fully transparent and enable accurate dynamic light scattering measurements, free from multiple scattering. In addition, static light scattering measurements have been performed with the same solutions in the absence of cross-linker (Al(III)). Because of the complexity of the problem, we will only discuss the results of very dilute xanthan solutions in order to have a reliable reference of the nongelling system.

The system analyzed here, i.e., xanthan in the presence of Al(III), is one which has recently undergone a detailed rheological characterization.[3] These findings are now extended in this paper, by considering light scattering results that provide information on the temperature of gelation (T_{gel}), and structural properties. Further information concerning translational and segmental motions is obtained from dynamic light scattering.

* To whom all correspondence should be addressed. Telephone: +61 3 8344 7440. Fax: +61 3 8344 4153. E-mail: d.boger@chemeng.unimelb.edu.au.
[†] University of Melbourne.
[‡] University of Freiburg.

10.1021/ma001706g CCC: $20.00
Published on Web 04/03/2001

Theoretical Background. This section is intended to only present the expressions of direct interest to discussion of DLS and SLS on gels. Although the dynamics of large scale molecules in solution are well-understood,[12] the dynamics associated with systems beyond a critical percolation threshold (the gel point) are still widely unknown and have been the subject of various approaches in terms of DLS, a concise version of which shall be presented here. It may be tempting to extrapolate the properties from the pregel beyond the critical limit where gelation takes place. The Flory−Stockmayer[19,20] and percolation[21] theories and their application to gelation show clearly critical behavior around the gel point with a discontinuity in molecular properties (M_w and R_g) and a disproportionation in a gel and a sol-fraction.[19,20] A solution that has passed through the percolation threshold (gel point) consists of a network that extends through the sample with quasi-solid-state behavior and also consists of *under*-critically extended clusters. *Under*-critically extended clusters suggests clusters that although large are (a) not part of the percolated network and (b) not extended enough to form a percolating network themselves. The same system prior to gelation consists of solely *under*-critically branched or cross-linked clusters with no equivalent infinite network. Consequently, the observed dynamics (in this work probed with DLS and SLS) differ markedly in the pregel and the gel states. The following consideration gives an overview of two theoretical approaches previously used to analyze time correlation functions (TCF) from gelling systems.

The amplitude $E(q,t)$ of the electric field of light scattered by a medium undergoing fluctuations $\rho(r,t)$ in concentration may be written in the continuous form as[12]

$$E(q,t) \sim \rho(q,t) = \int_v \mathrm{d}^3\mathbf{r}\, \rho(\mathbf{r},t) \exp[i\mathbf{q}\cdot\mathbf{r}] \qquad (1)$$

the scattered intensity as determined by light scattering experiments may be expressed as

$$I(q,t) = |E(q,t)|^2 \qquad (2)$$

From a single DLS measurement, an estimate of the *time-averaged* normalized time correlation function (TCF) of the scattered intensity $g_2^{\mathrm{T}}(q,\tau)$ is obtained:

$$g_2{}^{\mathrm{T}}(q,\tau) \equiv \frac{\langle I(q,0)I(q,\tau)\rangle_{\mathrm{T}}}{\langle I(q,0)\rangle_{\mathrm{T}}{}^2} \qquad (3)$$

For a system containing an infinite network or a "*frozen-in*" component, the electric field may be considered in terms of two components, a fluctuating component which is a zero mean Gaussian variable in the time domain and a constant time independent field. Thus, the time averaged scattering intensity may be expressed as[4,5,12,17]

$$\langle I(q)\rangle_{\mathrm{T}} = \langle I_{\mathrm{F}}(q)\rangle_{\mathrm{T}} + I_{\mathrm{C}}(q) \qquad (4)$$

where $I_{\mathrm{F}}(q,t)$ is the fluctuating and $I_{\mathrm{C}}(q)$ is the constant component. These are related to fluctuations in the electric field as $I_{\mathrm{F}}(q,t) = |E_{\mathrm{F}}(q,t)|^2$ and $I_{\mathrm{C}}(q) = |E_{\mathrm{c}}(q)|^2$. It was shown by Pusey et al.[4,23] and Geissler[5] that, by applying eqs 1−4, $g_2^{\mathrm{T}}(\tau)$ may be expressed as

$$g_2{}^{\mathrm{T}}(q,t) - 1 = \frac{\langle E_{\mathrm{F}}(q,0)E_{\mathrm{F}}{}^*(q,\tau)\rangle_{\mathrm{T}}{}^2 + 2I_{\mathrm{C}}(q)\langle E_{\mathrm{F}}(q,0)E_{\mathrm{F}}{}^*(q,\tau)\rangle_{\mathrm{T}}}{\langle I(q,0)\rangle_{\mathrm{T}}{}^2} \qquad (5)$$

For simplicity, an ideal spatial coherence factor $\beta = 1$ has been assumed. The spatial coherence factor depends on the quality of instrument calibration and optical setup and will be defined experimentally for our setup.

Up to this point, the two approaches to be considered in this paper, the *nonergodic* concept and the *heterodyne* approximation, theoretically are identical. It is now appropriate to consider these two approaches individually. Both concepts have been developed to deal with the erratic fluctuations thought to be associated with large scale heterogeneities that have in the past caused significant perplexity into how to reliably interpret these effects. Originally and until recently, it has been proposed to deal with gels by assuming a certain spatial homogeneity even beyond the percolation threshold.[7,22] Tanaka's theory assumes homogeneous gels. Near the gel point, however, the majority of material consists of under-critically cross-linked structures that will inevitably introduce a degree of heterogeneity. These will grow as the cross-linking proceeds because of the strongly diffusion inhibited reaction in the gel. Such heterogeneities and their erratic angular dependence (or spatial orientation) have a large effect on the scattered intensity[13−18] and consequently also on the correlation functions. The *nonergodic* approach suggests that, within a given time interval, all spatial configurations will not be realized, due to an effective *frozen-in* component, whereas the *heterodyne* approach suggests that the large scale inhomogeneities may be regarded as dynamically uninteresting features, that "heterodyne" with the gel network.

A detailed theoretical approach to the frozen heterogeneities in gels was recently developed by Panyukov and Rabin.[14] The theory is in a way an extension of the Tanaka theory by considering in addition to the solidlike elasticity the effect of a mobile, liquidlike component. The authors confined themselves to the static or equilibrium properties. They succeeded in a satisfactory description of the stunning observation by Bastide et al.[15] in the small-angle neutron scattering (SANS) from swollen and uniaxial extended gels. No attempt was made, however, to derive corresponding relationships for the dynamics. A qualitative approach was made by Shibayama.[18] A comparison of different experimental studies revealed that up to four apparent diffusion coefficients are to be distinguished, depending on the applied experimental method. The physical basis of this rather confusing outcome remains unresolved. Because of lack of time, we were not able to carry out a comprehensive study on the static properties and could make no comparison with this interesting theory (see also comments in the Discussion).

The starting positions for the two dynamic theories considered in this paper appear to be remarkably similar whereas the final result is significantly different.

Heterodyne Approach.[5] The time-independent variable (denoted in eq 4 with subscript C), may result from a small fraction of the primary beam, e.g. stray light from the optical system. $I_c(q)$ may also originate from very slowly moving large particles that appear to be

frozen-in when probed on a time scale less than that associated with the movement of such a heterogeneity. As mentioned above, the heterodyne approach considers these as dynamically uninteresting particles. After some arrangement of eq 5, one arrives at an expression for the normalized time correlation function $g_H(q,\tau)$ (where subscript H denotes heterodyne) may be solved:

$$g_H(q,\tau) = 1 + \frac{1}{X}\left[\sqrt{{g_2}^T(q,\tau) - ({g_2}^T(q,0) - 1)} - 1\right] \quad (6)$$

where $(1 - X)$ denotes the fraction of heterodyne contribution to the TCF. X is expressed as

$$X = \frac{\langle I_F(q)\rangle_T}{\langle I(q)\rangle_T} \quad (7)$$

and the TCF is

$$g_H(q,\tau) = \frac{\langle E_F(q,0)E^*{}_F(q,\tau\rangle_T}{\langle I_F(q)\rangle_T} \quad (8)$$

The parameter X is obtained from the value of the TCF at a delay time of zero, that is

$$X = 1 - \sqrt{2 - {g_2}^T(q,0)} \quad (9)$$

Nonergodic Approach.[4,23] The heterodyne approach is fully consistent if the scattering cell is not moved to another position. This suggests that only one spatial arrangement is observed, which may not be the same as all spatial averages, and in the case of a gel with a significant frozen in component the latter is the case. Since not all spatial orientations can be assumed to be realized, the Siegert relationship[24] also cannot be expected to hold. To obtain a self-consistent result over an entire sample, it is necessary to conduct ensemble averaging from many different sample spaces (for example by stepwise rotation of the sample cell). Theoretically, the nonergodic approach requires correlation functions from all possible spatial configurations (i.e., infinite number of positions). Generally 100−150 sample positions are considered statistically sufficient. (Some works report up to 2000 positions.[17]) If, for an arbitrary nonergodic medium a statistically significant number of spatial orientations are measured, then one has for the fluctuating field:

$$\langle E_F(q,0)E_F^*(q,\tau)\rangle_T = \langle E_F(q,0)E_F^*(q,\tau)\rangle_E \quad (10)$$

The notation $\langle ...\rangle_E$ represents an ensemble average that is an approximation to all possible spatial configurations. The right side of eq 10 can be related to the normalized TCF, ${g_1}^E(q,\tau)$, by

$$\langle E_F(q,0)E_F^*(q,\tau)\rangle_E = \langle I(q)\rangle_E \times [{g_1}^E(q,\tau) - {g_1}^E(q,\infty)] \quad (11)$$

At the zero time limit eq 11 reduces to

$$\langle I_F(q)\rangle_T = \langle I(q)\rangle_E[1 - {g_1}^E(q,\infty)] \quad (12)$$

and then by some rearrangement we can describe the normalized TCF by

$$g_E(q,\tau) = 1 + \frac{1}{Y}\left[\sqrt{{g_2}^E(q,\tau) - ({g_2}^E(q,0) - 1)} - 1\right] \quad (13)$$

where

$$Y = \frac{\langle I(q)\rangle_E}{\langle I(q)\rangle_T} \quad (14)$$

Note the difference between eq 6 and eq 13 consists only in the normalization described by X and Y in eqs 7 and 14, respectively. Pusey et al.[23] related in his fundamental paper ${g_2}^E(q,\tau)$ also to the normalized *nonergodic* time correlation function using the well-known Siegert relationship[24]

$${g_2}^E(q,\tau) = 1 + |\beta g_E(q,\tau)|^2 \quad (15)$$

which appears to be justified, as by the applied technique now the spatial fluctuations are taken into account. Here β is the experimentally determined spatial coherence factor, determined in the present study as $\beta = 1.04 \pm 0.02$ using a standard, dilute polystyrene latex solution for our experimental setup.

Now the remarkable similarity of the final result of both the *nonergodic* and the *heterodyne* approach can be discussed. Although eqs 6 and 13 exhibit formal similarity they include very different interpretations due to the difference in definition of X and Y presented in eqs 8 and 14. The heterodyne approach considers large-scale inhomogeneities as uninteresting and as a result the intermediate scattering function will decay completely to zero. The nonergodic approach takes into account all features and comprises objects which move on time scales that are beyond the length of the measurement. These are considered as effectively *frozen-in*, resulting in an intermediate scattering function that decays to a nonzero value beyond the percolation threshold. This paper presents data by using both the heterodyne and the nonergodic approach. We will clarify where these techniques should agree, and where inherently they are expected to differ.

Static Properties. Static light scattering may be applied to dilute solutions for determining the molecular weight of individual chains and the radius of gyration. The light-scattering data are normally analyzed from standard Zimm plots[25,26] according to the well-known equations

$$\frac{Kc}{R_\theta} = \frac{1}{M_w}\left(1 + \frac{{R_g}^2q^2}{3} - ...\right) + 2A_2c + ... \quad (16)$$

with

$$q = \frac{4\pi n_o}{\lambda_o}\sin\left(\frac{\theta}{2}\right) \quad (17)$$

where K is the optical contrast factor, which depends on the difference in the refractive indices of the solution from the solvent, R_θ the Rayleigh ratio of scattered intensities, λ_o the wavelength of light used in a vacuum, n_o the refractive index of the medium, and θ the scattering angle. For branched structures, the Berry[27] plot ($(Kc/R_\theta)^{1/2}$ vs $q^2 + kc$) may more adequately be used, because it often removes much of the curvature observed in the angular dependence of the Zimm plot. If the structure is expected to be large and globular, as might be the case for aggregates of xanthan, the Berry plot is not linearized but still shows an upturn. In these cases it is often appropriate to apply a modified Guinier[28] plot,

i.e., ($\ln(Kc/R_\theta)$ vs $q^2 + kc$) that removes the upturn even more efficiently. From these plots the molar mass M_w, radius of gyration R_g, and the second virial coefficient A_2 are obtained in the usual manner as described in textbooks on light scattering.[29] From the limiting curve of the angular dependence at zero concentration, the particle scattering factor, $P(q)$ is obtained and is given as

$$P(q)^{-1} = \left[\frac{Kc}{R_\theta}\right] / \left[\frac{Kc}{R_\theta}\right]_{q=0} = R_{\theta=0}/R_\theta \qquad (18)$$

A plot of the reciprocal particle scattering factor against $u^2 = q^2R_g^2$ results in curves with initial slope of $^1/_3$, independent of the particle shape. Deviations observed at large u^2 are characteristic of the various architectures.

Experimental Section

Xanthan gum is a high molecular weight extracellular polysaccharide produced by bacteria of the genus X*anthomonas*. Commercial xanthan gum is extracted from *Xanthomonas campestris*; however, for the purpose of most scientific studies, it is extracted from *Xanthomonas phaseoli* and *Xanthomonas juglandis*. Xanthan gum chemically is considered as an anionic polyelectrolyte, with a backbone chain consisting of (1→4)*β*-D-glucan cellulose. The polymer backbone is substituted at C-3 on alternate glucose residues with a trisaccharide side chain. The side chain consists of *β*-D-mannopyranosyl-(1→4)-(α-D-glucuropyranosyl)-(1→2)-*β*-D-mannopyranoside 6-acetate. A pyruvic acid residue is linked to the 4 and 6 positions on between 31% and 56% of the terminal D-mannose residues.[30−32]

The polysacharide is water-soluble and was dispersed in 5 mg/mL (85 mmol) NaCl at room temperature by gentle shaking for 24 h. Following this, it was stored at 4 °C to reduce bacteria growth. All samples were used within 5 days of preparation. Deionized water was used for the preparation of all solvent solutions and was filtered three times through an Anotop filter (Merck), pore size 0.02 μm. Xanthan concentrations in the presence of NaCl were prepared in the range 0.02−0.2 mg/mL. Prior to measurement the samples were filtered once through a 5.0 μm filter and then 3 times through a 0.8 μm filter—the last time into 8 mm internal diameter light-scattering cells. All cells were acid/base washed prior to being washed for at least 20 min in an acetone fountain.

Preparation of the xanthan−Al(III) gelling systems involved dispersion of 1.11 mg/mL xanthan in 5 mg/mL NaCl. Al(III) solutions were prepared at 28 mg/mL from an $Al_2(SO_4)_2 \cdot 16H_2O$(aq) source and were filtered three times through a 0.2 μm filter. Directly prior to use, the xanthan solution was filtered through a 5.0 μm filter twice. The Al(III) solution was added in the ratio 1:9, while being retained at 15 °C, and stirred gently. The resultant solutions, 1.0 mg/mL xanthan and 280 ppm Al(III), were then stored at 4 °C. The cold solution was filtered once through a 0.8 μm filter directly into the light-scattering cells before measurement.

Static light-scattering (SLS) measurements were performed using a modified computer controlled SOFICA photogoniometer (G. Baur, Intrumentbau, Hausen, Germany), that was equipped with a 2 mW HeNe laser ($\lambda_o = 632$ nm). Measurements were made in the angular range 30−150° in steps of 5°. Temperature regulation was available between 10 and 65 °C ± 1.0 °C.

Dynamic light-scattering (DLS) measurements were performed using an automatic ALV goniometer and an correlator ALV 5000 (ALV, Langen, Germany). For all experiments the correlator was operated in "log mode", enabling 192 channels to be spaced logarithmically with time and thus enabling up to 9 decades of time to be analyzed. A krypton-ion laser (red) with a wavelength of $\lambda_0 = 647.1$ nm and an argon-ion laser (blue) with wavelength $\lambda_0 = 488$ nm were used as light sources. Monomode fiber optics were used. The temperature in the light scattering experiments was regulated by an external temperature-control for the refractive index matching bath, containing the light-scattering cells. Temperature regulation was available between 15 and 90 °C ± 0.2 °C. The angular dependence was recorded from 30 to 120° in steps of 10°.

Systems where the time average of the scattering intensity $\langle I(q)\rangle_T$ deviated from the corresponding ensemble average $\langle I(q)\rangle_E$ were denominated as *nonergodic*.[4,23] This observation suggested a procedure of measuring the ensemble averaged intensity ($\langle I(q)\rangle_E$) separately. To determine $\langle I(q)\rangle_E$ the count rate was evaluated over a period of between 40 and 120 s. The sample was then rotated 3.3° by a stepping motor and the procedure was repeated between 100 and 500 times. A probability distribution was obtained that together with $g_2^T(q,\tau)$ allows determination of both $\langle I(q)\rangle_E$ and $\langle I(q)\rangle_T$ and then calculation of $g_E(q,\tau)$ from eq 13 and eq 14. Alternatively, $g_2^E(q,\tau)$ was measured directly by collection of the individual time correlation functions at each sample position, for 40 s and over 100 sample positions. The total time correlation function, $g_2^E(q,\tau)$ is a collection of a minimum of 100 runs, normalized for the number of photons and the number of summations. From $g_2^E(q,\tau)$, as has been suggested previously,[23] the intermediate scattering function, $g_E(q,\tau)$, may be calculated directly from the Siegert[24] relationship. Both techniques for collection of $g_1^E(q,\tau)$ will be compared in the Results section.

For all temperature-dependent measurements, a thermal equilibrium time of 40 min was chosen. Measurements were conducted at $q^2 = 3.35 \times 10^{10}$ and 5.88×10^{10} cm^{-2} for the red and blue light sources, respectively (These q values correspond to $\theta = 90°$ on both instruments. The nonergodic approach was conducted only on the red laser at $q^2 = 3.35 \times 10^{10}$ cm^{-2}. Angular dependent measures were made deep in the gel and the liquid states at 72 and 15 °C, respectively. At low temperatures (before the sample was gelled), the systems were observed to be predominantly ergodic within experimental error.

DLS and SLS of Xanthan in the Absence of Cross-Linker—Results and Discussion

Static Light Scattering. Before considering xanthan−Al(III) gels, the static and dynamic behavior of xanthan solutions was characterized. The xanthan used in this work was taken as a dry powder and was not heat-treated or dialyzed to a single salt form. Therefore, the molecular properties obtained from these solutions will be indicative of those for many of the industrial applications of xanthan gum. All solutions discussed in this section were prepared in 5 mg/mL NaCl. Figure 1 illustrates a modified Guinier plot of xanthan in 5 mg/mL NaCl as measured at room temperature. The very large values of M_w(1410 × 10^6 g/mol) and R_g (409 nm) suggests that xanthan is present in aggregates. On the basis of an approximate molar mass of individual molecules of 3.5 × 10^6 g/mol as measured in the literature[33−36] and determined by SEC−MALS (size exclusion chromatography−multiangle light scattering), there are approximately 600 molecules in these aggregates. Upon heat treatment, a significant change in the structural properties of xanthan solutions was found by others,[33,34] Figure 2 illustrates a Guinier plot for the same system as described in Figure 1 after heat treatment at 130 °C and 2 bar for 40 min. The molar mass decreased by a factor of more than 10 to $M_w = 79 \times 10^6$ g/mol) accompanied by a less pronounced decrease of the dimensions to $R_g = 315$ nm.

To obtain more information on the strucutral properties of the aggregates, it is appropriate to present the particle scattering function in a Casassa−Holtzer[37,38]

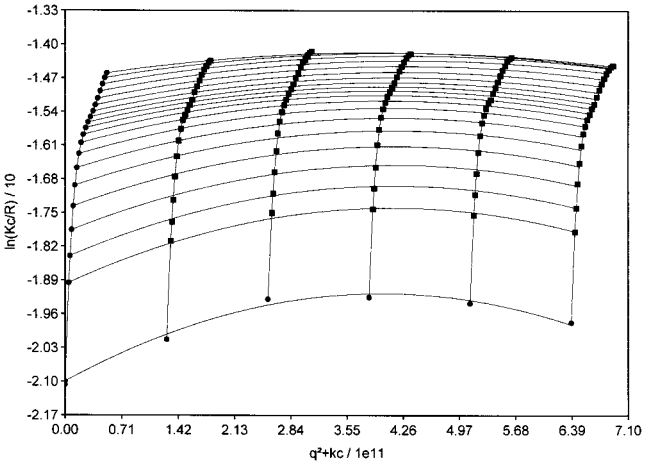

Figure 1. Modified Guinier plot (i.e., $\ln(Kc/R_\theta)$ against $q^2 + kc$) of xanthan in 5.0 g/L NaCl measured at 20 °C with no heat treatment. $M_w = 1410 \times 10^6$ g/mol, $R_g = 409$ nm, and $A_2 = 1.03 \times 10^{-5}$ mol/mL/g^2. Fourth-order fit in concentration and second-order fit in q^2. $c^* = 1/(A_2M_w) = 0.06$ mg/mL, where c^* is the overlap concentration.

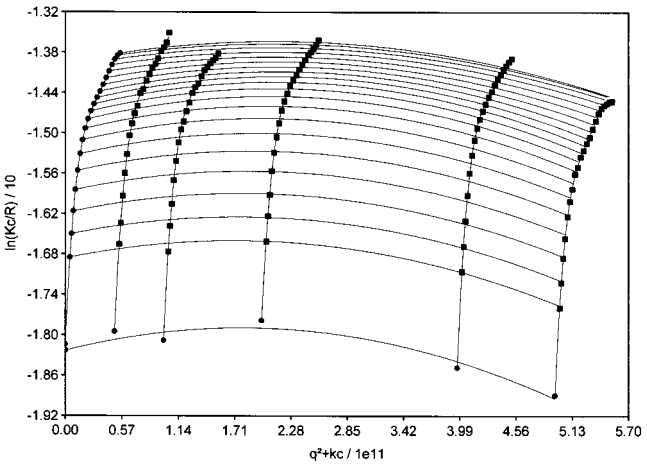

Figure 2. Modified Guinier plot of xanthan in 5.0 g/L NaCl measured at 20 °C after heat treatment at 130 °C and 2 bar for 40 min. $M_w = 78 \times 10^6$ g/mol, $R_g = 315$ nm, and $A_2 = 4.59 \times 10^{-5}$ mol/mL/g^2. Fourth-order fit in concentration and second-order fit in q^2. $c^* = 0.24$ mg/mL.

plot, i.e., $(qR_g)R(q)/Kc$ against qR_g, as illustrated in Figure 3. The solid line is a spline fit at high values of $u = qR_g$ where R_g was found from the initial slope in the Guinier plot according to eq 16. From the plateau height at large u values the molar mass per unit length, $M_L = M/L$ may be estimated. For the xanthan systems presented here M_L was determined as 28 900 and 10 460 g/(mol nm) without and with heat treatment, respectively. On the basis of the molar mass per unit length for individual xanthan molecules ($M_L = 1830$ g/(mol nm),[33,39] the data in Figure 3 corresponds to bundles of 16 pairs of chains in the absence of heat treatment, which is significantly reduced to 6 pairs of chains after heat treatment. The less pronounced decrease in R_g from 409 to 315 nm is in agreement with a model for branched bundles of xanthan molecules. After heat treatment, the bundles contain less chains, but the overall degree of branching and thus overall size are not as affected. Further evidence for this structure my be seen by considering the Krakty plot[40] as illustrated in Figure 4 for xanthan without heat treatment. Previously, a number of form factors have been derived for various polymer architectures. For a polydisperse ran-

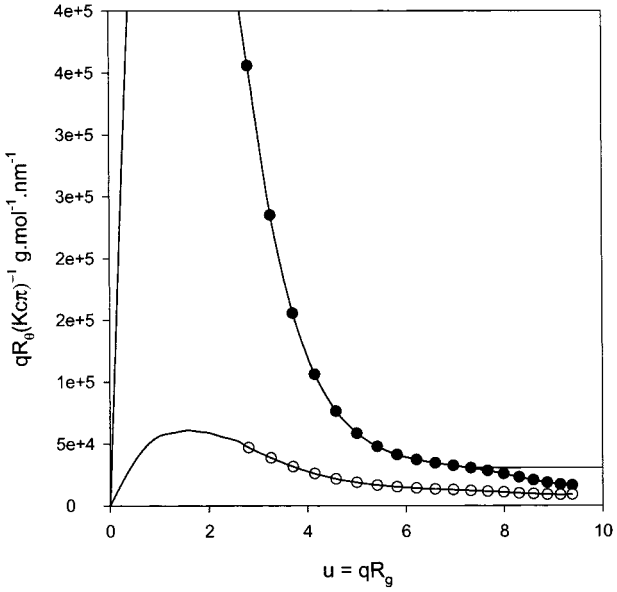

Figure 3. Casassa−Holtzer plot of xanthan in 5 mg/mL with and without heat treatment as desribed in Figures 1 and 2: (closed circles) no heat treatment; (open circles) heat treatment. The solid-line represents a spline curve of best fit through the data which is extrapolated at low u values to the universal relationship for all systems described in eq 19.

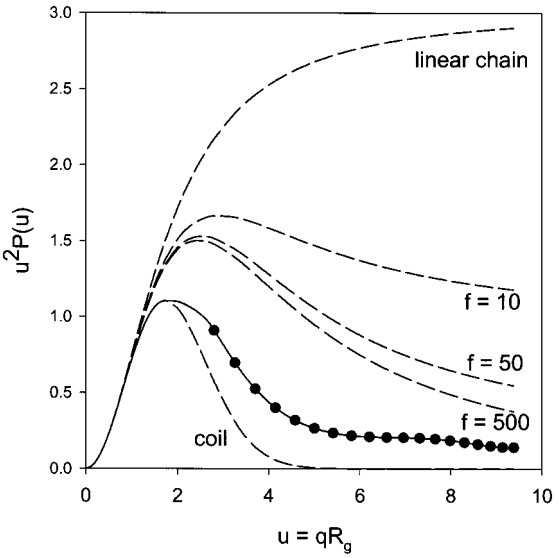

Figure 4. Kratky plot of xanthan in 5 mg/mL NaCl without heat treatment. Solid line and data points represent data and extrapolated data presented in Figure 3. Other lines represent form factors (from top to bottom) for polydisperse linear chains, polydisperse star molcelules with $f = 10$, 50, and 500 arms and polydisperse spheres which are described by the Guinier approximation.

dom coil of linear flexible chains, Zimm predicted[25]

$$P(\theta) = \frac{1}{1 + u^2/3} \tag{19}$$

which, as expected, does not describe the system well (Figure 4). Also a starlike structure with f polydisperse flexible arms[41]

$$P(\theta) = \frac{1 + u^2/3f}{[1 + u^2(f + 1)/6f]^2} \tag{20}$$

did not correctly represent the measurement. In fact,

the Casassa−Holtzer[37,38,42] plot suggests that the branched bundles in the structure have considerable rigidity. Such structure requires a more sophisticated fit with a complex form factor that is considered to be beyond the scope of this work (although it may be considered in future work by computations methods currently being developed).[43]

Dynamic LS. Further evidence for a branched/globular structure is obtained from the translational mobility of the molecules as determined by dynamic light scattering. The solutions of xanthan gum show ergodic, or homodyne, behavior, this is evidenced by both the complete decay of $g_2^T(q,\tau)$ to a baseline of unity as well as an apparent normal distribution of the time averaged intensities $\langle I(q)\rangle_T$, which will be commented upon in more detail in the following section. Applying the Siegert[24] relationship, the intermediate field scattering function, $g_T(q,\tau)$ was obtained. The TCF, $g_T(q,\tau)$ could be well described by a Kohlrausch−William−Watts (KWW) stretched exponential function:[44,45]

$$g_T(t) = A \times \exp\left[-\left(\frac{t}{\tau}\right)^{\beta}\right] + C \qquad (21)$$

where $A \approx 1$ and $C \approx 0$ are constants corresponding to the correlation strength and a very small nonzero plateau as a result of a possible small nonergodic contribution. The two other parameters τ and β characterize the mean relaxation time $\langle\tau\rangle$ given as

$$\langle\tau\rangle = \left(\frac{\tau}{\beta}\right)\Gamma(\beta^{-1}) \qquad (22)$$

where $\Gamma(x)$ is the gamma function. Also a two-mode KWW fit was tested, but the amplitude of the contribution of the second apparent diffusion mode was low. The increased number of variables introduced by a two-mode KWW fit, would not be justified by the small contribution of the second mode.

Extrapolating the angular dependent apparent diffusion coefficient $D_{app}(q) = 1/(\langle\tau\rangle q^2)$ to zero scattering angle, the mutual diffusion coefficient $D_{mut}(c)$ is obtained. Extrapolation of $D_{mut}(c)$ to $c \rightarrow 0$ results in the translation diffusion coefficient $D_{trans} = 3.15 \times 10^{-9}$ cm^2/s (Figure 5). Applying the Stokes−Einstein relationship, one finds a hydrodynamically effective radius $R_h = 909$ nm according to

$$D = \frac{kT}{6\pi\eta_s R_h} \qquad (23)$$

where k is the Boltzmann constant and η_s is the solvent viscosity. The ratio of the radius of gyration and the hydrodynamic radius ($\rho = R_g/R_h$) was previously found to be characteristic of molecular structure.[46] For the present system, $\rho \cong 0.45$ was derived, which is below that for impenetrable spheres ($\rho = 0.778$) yet remarkably similar to that observed for "microgel type structures" containing many dangling ends ($\rho = 0.35$–0.55).[26,47]

From the combination of static and dynamic light scattering studies, it becomes clear that with filtration, aggregated xanthan structures remain preserved or reform. The results indicate that the aggregates are branched structures containing fairly rigid bundles and many dangling chain ends. No additional estimate of the number of aggregates and of the precise structure was made for filtered xanthan in the absence of cross-linker.

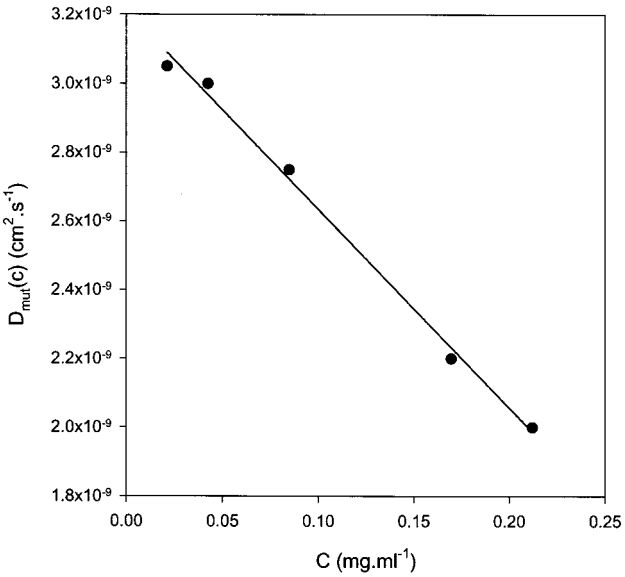

Figure 5. Concentration dependence of the mutual diffusion coefficient $D(c)$ for xanthan solutions in 5 mg/mL NaCl. Data shown here had no heat treatment and all measurements were made at 20 °C. Solid line represents a linear fit of the data, from which an extrapolated zero concentration value was determined as $D_{q=0,c=0} = 3.15 \times 10^{-9}$ cm^2/s, corresponding to a hydrodynamic radius of $R_h = 909$ nm.

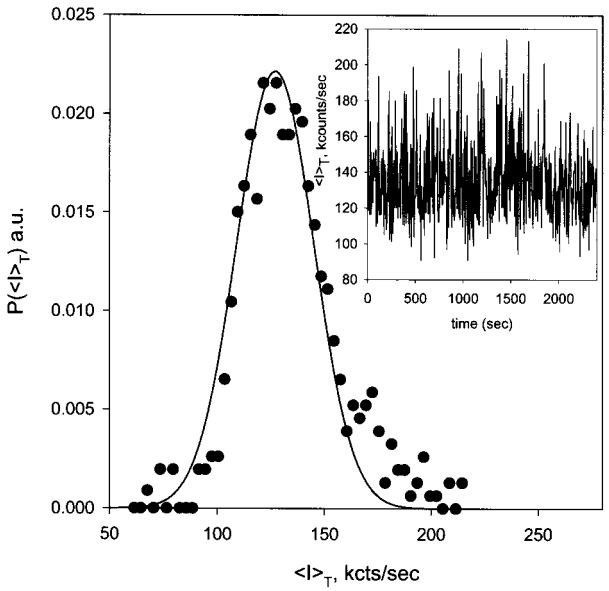

Figure 6. (a) Frequency distribution (histogram) of $P(\langle I(q)\rangle_T)$ for 1.0 g/L xanthan and 2.8 g/L Al(III) as measured at 30 °C (liquid) and a scattering angle of $\theta = 90°$. $\lambda_o = 647$ nm. (b) Inset representing $\langle I(q)\rangle_T$ vs time that was the basis for the calculation of $P(\langle I(q)\rangle_T)$.

DLS and SLS Studies of Xanthan−Al(III) Gelling System−Results

Time-Average Intensities. The particular behavior of the gel system became apparent directly from observation of the time averaged scattered intensity as a function of time for one scattering angle and at one sample position. Figure 6 illustrates $\langle I(q)\rangle_T$ as a function of time for the system in the sol regime, i.e., at 30 °C, whereas Figure 7 illustrates $\langle I(q)\rangle_T$ at 57 °C which is

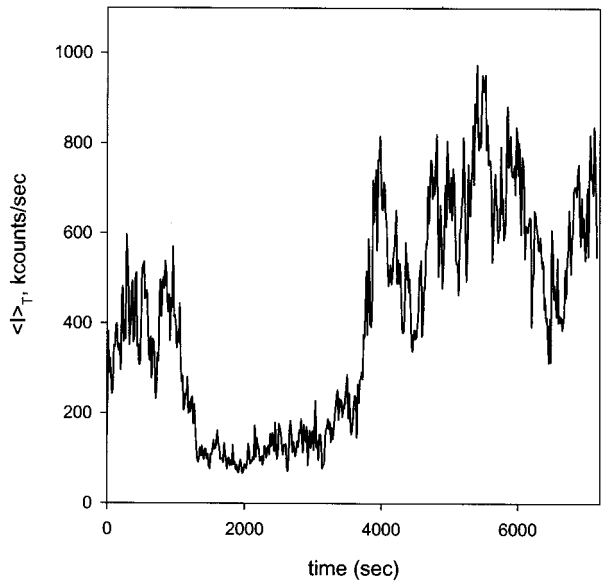

Figure 7. $\langle I(q)\rangle_T$ vs time for 1.0 g/L xanthan and 2.8 g/L Al-(III) as measured at 57 °C (gel) and scattering angle $\theta = 90°$. $\lambda_o = 647$ nm.

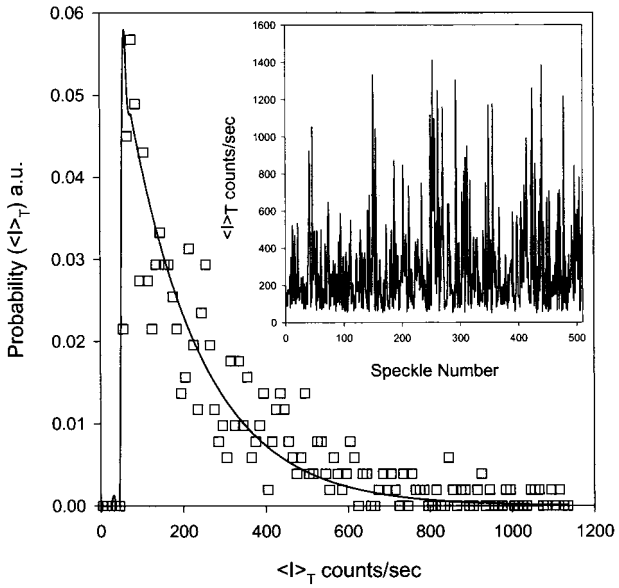

Figure 8. (a) $\langle I(q)\rangle_T$ for various sample positions obtained by rotating the sample 520 times and taking an averaged intensity over 40 s for each measurement Data taken from 1.0 g/L xanthan and 2.8 g/L Al(III) as measured at 57 °C (gel) and at $\theta = 90°$. $\lambda_o = 647$ nm. (b) Frequency distribution, $P(\langle I(q)\rangle_T)$, of the data given in part a. The solid line represents a least-squares fit of eq 27. Analysis gives $\langle I(q)\rangle_F = 45$ kcounts/s and $\langle I(q)\rangle_E = 218$ kcounts/s. See also ref 12.

deep in the gel state. As a liquid, the system shows large fluctuations in the scattered intensity. However, over relatively short time periods, $\langle I(q)\rangle_T$ follows a Gaussian distribution in time (see inset in Figure 6). Contrary to this, deep in the gel state, $\langle I(q)\rangle_T$ shows significant fluctuations over very long time scales (2 h) indicating an enormous decrease of speckle mobility (Figure 7). In the gel state, the total intensity results from two components, an ensemble averaged intensity that is time independent $\langle I(q)\rangle_E \cong I_C(q)$ and a time average of the fluctuating component $\langle I_F(q)\rangle_T$ (see eq 4). The time average intensity $\langle I(q)\rangle_T$ at a particular position is considered to remain constant over a period of minutes; however, over very long time scales it will vary. Figure 8 illustrates $\langle I(q)\rangle_T$ gathered over 500 sample positions for a period of 40 s at each position, showing clearly a constant baseline and significant fluctuating component. For non-crosslinked systems, $\langle I(q)\rangle_T$ is the same for all scattering positions and equal to $\langle I(q)\rangle_E$ or Gaussian in time as shown in Figure 6. From the data presented in Figure 8, a probability histogram is constructed by grouping the data into intervals of 5 kcounts/s, enabling the calculation of a probability distribution function $P(\langle I(q)\rangle_T)$ of the scattered intensity $\langle I(q)\rangle_T$ sampled over all ensembles. The probability distribution function, shows a cutoff at low $I(q)$ resulting from the contribution of $\langle I(q)\rangle_F$. In addition, an exponential decay in the frequency or large scattering intensities is observed as was previously predicted by Pusey et al.[4,23] The probability distribution function was shown to obey the relationship[17]

$$P(\langle I(q)\rangle_T) \sim H(\langle I(q)\rangle_T - \langle I(q)\rangle_F) \exp\left[-\frac{\langle I(q)\rangle_T - \langle I(q)\rangle_F}{\langle I(q)\rangle_E - \langle I(q)\rangle_F}\right] \quad (24)$$

where $H(x)$ is the Heaveside function, with $H(x) = 0$ for $x < 0$ and $H(x) = 1$ for $x > 0$. In deriving eq 24, the authors assumed that each $\langle I(q)\rangle_T$ comprises of many decay times representing the fast fluctuations in the system and in addition from nonmoving speckles. The solid line in Figure 8 represents a linear regression of eq 24 to the data. From the fit, we found $\langle I(q)\rangle_F = 45$ kcounts/s and $\langle I(q)\rangle_E = 218$ kcounts/s, giving a ratio of $r = \langle I(q)\rangle_F / \langle I(q)\rangle_E \cong 0.2$. Previous to us, Joosten et al.[17] observed a similar result for the more ideal gelling system of cross-linked polyacrylamide with $\langle I(q)\rangle_F = 7$ kcounts/s and $\langle I(q)\rangle_E = 11.7$ kcounts/s, giving a ratio of $r \cong 0.6$. The observed considerably lower scatter in intensity is a result of less heterogeneity of the gel that was built from cross-linked flexible polyacrylamide chains.

Recently Panyukov and Rabin[14] (PR) published a detailed and important theoretical treatment of the scattering behavior from inhomogeneous networks and swollen or uniaxial deformed gels. They showed that both the static density inhomogeneities ($\langle I_C(q)\rangle_E$) and the liquidlike fluctuations ($\langle I_F(q)\rangle_E$) have a rather complex angular dependence. Only in the asymptotic, far-q region ($qR_g \gg 1$) was a fairly simple and universal behavior found. The latter results from the fact that the scattering intensity from the large speckles decreases sharply proportional to q^{-4}. In general, however, the ratio $\langle I_F(q)\rangle_E / \langle I_C(q)\rangle_E$ has a strong and very complex angular dependence that is determined by the sizes (R_g and ξ) and amounts of the density inhomogeneities and the liquidlike fluctuating structures (i.e., the mesh size and the fluctuating amplitude of the corresponding chains). The evaluation of the PR functions in terms of structural parameters requires measurements over the whole q region of static light scattering which was beyond our capabilities, because of the long time that would be needed with our setup. In our study we measured the behavior only for one certain gel state at a fixed scattering angle of $\theta = 90°$.

Dynamic LS Experiments. Next an ensemble average intensity correlation function $g_2^E(q,\tau)$ was collected by 100 sample rotations over 4 h and compared with a time averaged intensity correlation function, $g_2^T(q,\tau)$ that was collected over 2 h in one sample position. Both

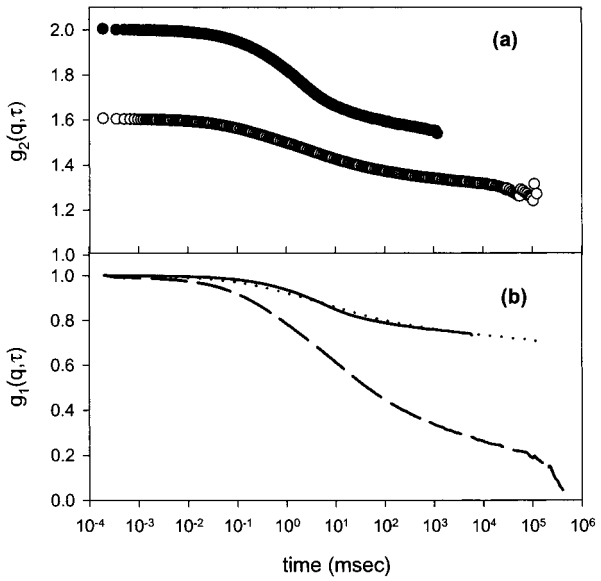

Figure 9. (a) Ensemble average intensity correlation function $g_2^E(q,\tau)$ (closed circles) and time-averaged intensity correlation function $g_2^T(q,\tau)$ (open circles) obtained for 1.0 mg/mL xanthan and 2.8 mg/mL Al(III) after equilibration at a scattering angle of $\theta = 90°$. $g_2^E(q,\tau)$ was averaged over 100 sample rotations with data collected for 40 s at each position. $g_2^T(q,\tau)$ collected over 2 h at 1 sample position. $\lambda_o = 647$ nm. (b) Intermediate scattering functions $g_1(q,\tau)$. Full line: calculated from $g_2^E(q,\tau)$ and eq 15. Dotted line: calculated from eq 13 and the data of $g_2^T(q,\tau)$ and analysis by eq 15 to obtain to give $\langle I(q)\rangle_E$ and Y. Dashed line: calculated from eq 8 and the data of $g_2^T(q,\tau)$. X calculated using eq 9 from the $\lim_{\tau\to 0} g_2^T(q,\tau)$ illustrated in part a.

measurements were made at 57 °C. The results of the ensemble average and time averaged correlation functions are presented in Figure 9a, illustrating clearly the nonequivalence of the two correlation functions. Such a result is expected for a nonergodic medium, and it would be clearly incorrect to assume the two to be equal. A similar test was conducted deep inside the liquid stage before the onset of gelation and equivalence of $g_2^E(q,\tau)$ and $g_2^T(q,\tau)$ within experimental error was observed indicating $\langle I(q)\rangle_T = \langle I(q)\rangle_E$, characteristic of an ergodic medium. Theoretically, the spatial coherence factor β should be 1.00, which is slightly lower than the 1.02 actually determined for an ergodic medium. The difference is a result of unavoidable errors in the optical alignment. The ensemble average correlation function $g_2^E(q,\tau)$, collected over 100 sample positions can be simply converted to the intermediate scattering function, $g_E(q,\tau)$ using the Siegert relationship (eq 15). The time average correlation function $g_2^T(q,\tau)$ can also be converted to the ensemble average intermediate scattering function by eq 13, where Y is calculated using $\langle I(q)\rangle_E$ from the above procedure and $\langle I(q)\rangle_T$ from the experiment. Figure 9b illustrates a remarkable agreement between the two procedures. Additionally, $g_2^T(q,\tau)$-can be converted to the intermediate particle scattering function via the heterodyne approach using eq 7 where X was obtained from the intercept (see eq 9). Figure 9b shows a much steeper initial decay for the heterodyne approach. In this experiment $X = 0.37 \pm 0.08$, whereas in the nonergodic approach $Y = 0.53 \pm 0.04$ was obtained. Note: the difference arises from different normalization in both types of experiments. Clearly no cumulant fit can be applied to the nonergodic TCF because such a fit requires a TCF that by definition has to decay to zero. Interestingly almost the same TCF is

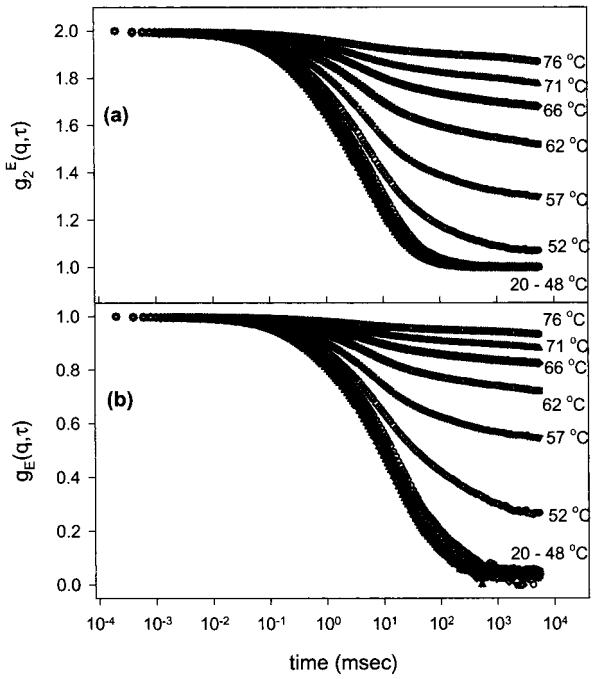

Figure 10. (a) $g_2^E(q,\tau)$ for 1.0 mg/mL xanthan and 2.8 mg/mL Al(III) for a range of temperatures. Data collected at a scattering angle of $\theta = 90°$ and $\lambda_o = 647$ nm. 100 sample rotations with a sample collection time of 40 s per rotation and 30 min thermal equlibration between temperatures. (b) $g_1^E(q,\tau)$ for 1.0 mg/mL xanthan and 2.8 mg/mL Al(III) for a range of temperatures. Data collected as described in part a.

obtained for $g_E(q,\tau)$ when the plateau value $g_E(q,\tau)$, is renormalized to zero.

Temperature Dependence of Dynamic LS Experiments. Experiments similar to those discussed above were conducted simultaneously on two different instruments ($\lambda_o = 496.5$ nm and 647 nm). For the one instrument ($\lambda_o = 647$ nm), it was possible to collect data from all spatial orientations (100 rotations), enabling nonergodic analysis; on the other instrument, $\lambda_o = 496.5$ nm, only one spatial orientation was probed, with a much longer collection period. The results of the ensemble average and time average correlation functions for a range of temperatures are presented in Figures 10 and 11, respectively. The difference between the two techniques is primarily that with the nonergodic approach $g_2^E(q,\infty)$ is seen to increase above 1 as the gelation proceeds (see Figure 10), whereas with the heterodyne approach, or the collection of a single spatial ensemble, $g_2^T(q,0)$ is seen to decrease below 2 as gelation proceeds (see Figure 11). Although $g_2^E(q,\tau)$ can be converted directly to the intermediate scattering function via the Siegert relationship (eq 15), the heterodyne approach requires X to be first calculated from the intercept, and then eq 7 can be applied. The intermediate scattering functions are illustrated in Figure 10b and Figure 11b. Two approaches were used to determine the mean relaxation times $\langle\tau\rangle$ from these data. For the nonergodic approach a two-mode KWW fit[43,44] according to eq 25 was found to provide a significantly better regression over all temperatures than the single mode of eq 22.

$$g_1^T(t) = A \times \exp\left[-\left(\frac{t}{\tau_1}\right)^{\beta_1}\right] + B \times \exp\left[-\left(\frac{t}{\tau_2}\right)^{\beta_2}\right] + C \tag{25}$$

As expected, the constant C was found to be $C > 0$ from

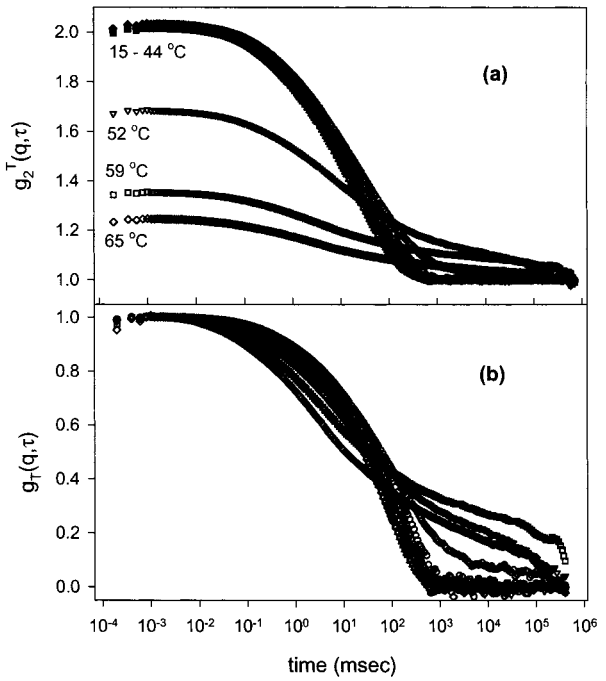

Figure 11. (a) $g_2^T(q,\tau)$ for 1.0 mg/mL xanthan and 2.8 mg/mL Al(III) for a range of temperatures. Data collected at a scattering angle of $\theta = 90°$ and $\lambda_o = 488$ nm with a collection time of 40 min before gelation and 2 h after gelation. (b) $g_1^T(q,\tau)$ for 1.0 mg/mL xanthan and 2.8 mg/mL Al(III) for a range of temperatures. Data collected as described in part a.

the frozen-in component. For the heterodyne analysis ($g_1^T(q,\tau)$), a two-mode KWW function was also used; however, in this case $C = 0$ was assumed, due to the exclusion of the frozen-in component. The results of this analysis will be considered in detail in the Discussion section.

Angular Dependence before and after Gelation. Although measuring the angular dependence for both approaches before, after, and during the gelation process would be optimal, the immense time required makes this experimentally unfeasible. The angular dependence of diffusing modes, both deep in the gel and in the liquid state, are however of great interest and have been obtained. The angular dependence was measured in the liquid state ($T = 15$ °C and $C = 0.05 \pm 0.01$) and deep in the gel state ($T = 72$ °C and $C = 0.90 \pm 0.05$) for angles $\theta = 30-120°$ for the same system presented above (1.0 mg/mL xanthan and 2.8 mg/mL Al(III) in 5 mg/mL NaCl). Only the nonergodic technique of sample rotation was measured. The results were again analyzed by using the KWW stretched exponential function (eq 25) and are discussed in detail below.

DLS and SLS Studies of Xanthan−Al(III) Gelling System−Discussion

Nonergodic and Heterodyne Analysis of Dynamic LS Data. It is clear that, even beyond the gel point, the xanthan system contains translational modes with very long relaxation times of $\langle\tau\rangle > 10^{-1}$ s. The question now arises as to how the two approaches presented in the results section differ and to what extend they should agree. The observation in Figure 7 is important as it provides the basis for the explanation, of why the nonergodic analysis and the heterodyne analysis differ. For a long enough time, eventually, $\langle I(q)\rangle_T$ will follow a Gaussian distribution and then all modes can be differentiated in the correlation function. Additionally some of the relaxation processes will be effectively frozen-in such that $\langle\tau\rangle \rightarrow \infty$. For most gelling systems the required time for the observation of the very slow relaxation is far too long as to conduct real measurements with available autocorrelators[48] (compare also ref 13). Thus, the question arises how to deal with the presence of very slow diffusive modes and how to compensate for effectively frozen-in components. The heterodyne approach deals solely with time averages, and the analysis is based on a long time average plateau as a baseline. In this case the intermediate scattering function decays to zero. The nonergodic approach, on the other hand, takes the ensemble average as reference by making many measurements but on much shorter time scales. Different time averages are collected and divided by the number of runs. Those inhomogeneities that diffuse on a longer time scale than the measurement are hence considered as being "frozen in" and appear as a nonzero plateau in the intermediate scattering function. Clearly significant difference in the estimation of the long relaxation times must result from these two approaches. However, such deviations do not exist when the fast motions are measured.

Although the time correlation functions gathered by the two techniques (Figure 9a) determined are clearly different, it is possible to transform them to a single intermediate scattering function using the determined value of $\langle I(q)\rangle_E$ from the fit of eq 25 to the data of Figure 8a, as illustrated in Figure 9b. The slight variation in the two functions is a direct result of the inherent difference in the two measurement procedures. Each correlation function for the ensemble average was collected over a much shorter time scale (40 s) than that for the time average (2 h). Consequently, the correlation function calculated from the *time average* $g_2^T(q,\tau)$ will reach to a longer sample time than that derived from the *ensemble* average. The ensemble average assumes any process, relaxing on a longer time scale than the measurement, as being *frozen-in*. Therefore, some processes are possibly occurring between the limits of the two correlation functions and are causing the disagreement in the intermediate scattering functions (see also refs 48 and 49). Also presented in Figure 9b is the heterodyne analysis (dashed curve) which illustrates a significantly steeper initial decay in $g_1^T(q,\tau)$ and the absence of a frozen in component. A cumulant fit would now give a much smaller diffusion coefficient from the nonergodic treatment than from the heterodyne TCF. However, the relaxation time of the fast motion in both curves, as determined by the KWW procedure within experimental error still give the same result. Heterodyne analysis (eq 9) of the data in Figure 9 gave $X = 0.37 \pm 0.08$, whereas the nonergodic value is found $Y = 0.53 \pm 0.04$ using eq 14, again underlining the difference between the time and ensemble averages. It is instructive to compare X with the plateau height $g_1^E(q,\infty)$. Although the plateau could not be observed as clearly as was found previously for the more ideal polyacrylamide gel,[17] it is possible to estimate it as $g_1^E(q,\infty) = 0.61 \pm 0.10$ which agrees surprisingly well within experimental error with the heterodyne contribution $(1 - X) = 0.53 \pm 0.04$.

Nonergodic and Heterodyne Analysis for the Entire Temperature Range. It is now appropriate to make a comparison of the nonergodic and the heterodyne approach over the entire temperature range and

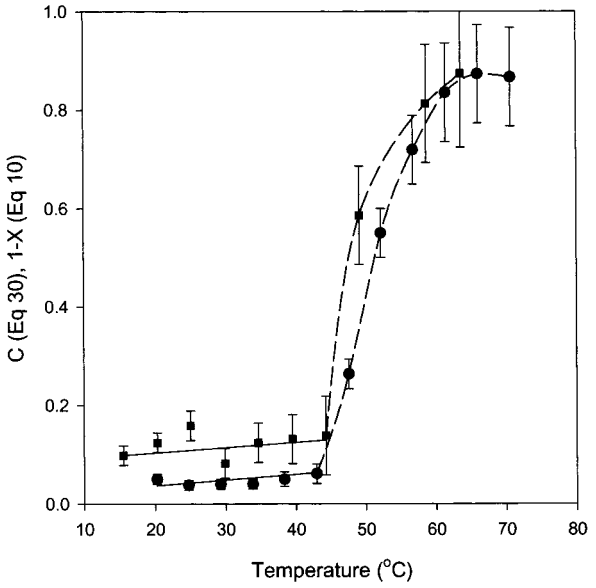

Figure 12. Results of KWW fit for (circles) C from eq 26 for $g_1^{E}(q,\tau)$. (squares) $(1 - X)$ determined by heterodyne analysis (eq 7) of $g_1^{T}(q,\tau)$. Full lines: linear regression of low-temperature data. Dashed curve: spline fit of data displaying significant nonergodic or heterodyne behavior.

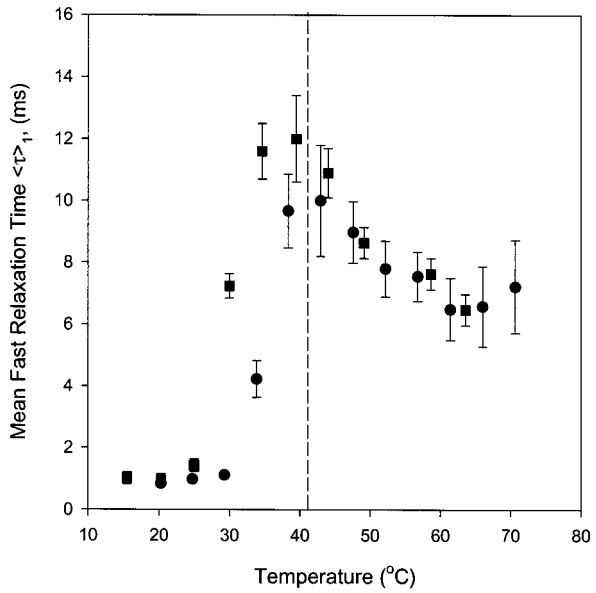

Figure 13. Mean fast relaxation times $\langle\tau\rangle_1$ (at 90°), for both the nonergodic approach (circles) and the heterodyne approach (squares).

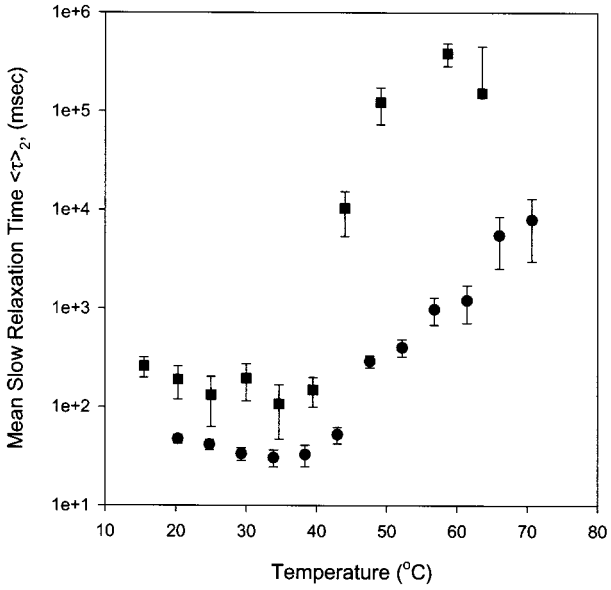

Figure 14. Mean slow relaxation times $\langle\tau\rangle_2$ (at 90°), for both the nonergodic approach (circles) and the heterodyne approach (squares).

thus through the gel point. The same analysis as employed for the data in Figure 9 was conducted at all temperatures for the data in Figures 10 and 11. Figure 12 compares the plateau constant C and heterodyne contribution $(1 - X)$. A remarkable agreement, within experimental error, was found over the entire gel process. The transition from a predominantly homodyne system to one with significant heterodyne contributions agrees satisfactorily with the temperature at which a transition from ergodic to nonergodic behavior is observed. Both experimental techniques indicate the transition to occur at 44 ± 2 °C, that may be interpreted now as the gel point. Although there is agreement within experimental error of C and $(1 - X)$ at $T > 44$ °C, these quantities may differ if the total time recording of $g_1^{T}(q,\tau)$ was significantly increased and more of the longer relaxation processes were accounted for in the correlation function. However, for permanent gels there will always be present a frozen-in component that in the nonergodic approach will result in a $C > 0$ and for the heterodyne approach in $X < 1$.

Previously, Joosten et al.[17] analyzed the intermediate scattering functions by considering the gel as both a nonergodic medium and a heterodyne scattering system. The authors concluded that the nonergodic medium consists of only one mean relaxation process that describes all concentration fluctuations and a second almost constant or frozen-in component that has a relaxation time $\langle\tau\rangle$ approaching ∞ when the cross-linking density is increased.[17] In the present system, the TCFs are in all cases best described by eq 25 with *two* mean relaxation processes and one frozen-in component. Figures 13 and 14 illustrate these fast and slow relaxation processes, respectively (calculated from eqs 25 and 21). The fast relaxation times display a significant maximum at $T = 44 \pm 2$ °C for both the nonergodic and the heterodyne approaches.

This maximum corresponds within experimental error to onset of heterodyne scattering that was taken as the gel point. This assignment allows a significant interpretation of the dynamic behavior of the fast mode. Following de Gennes' conception,[21] the increase in the relaxation time at low temperature is a sign of large cluster formation which increase with temperature as the gel point is approached. At the gel point, the translational diffusion should come to a complete standstill and consequently the relaxation time should diverge.[49] After the gel point, a network is obtained, and now the dynamics is governed by the mesh size of this network or, in the theory by Tanaka,[7] by the collective diffusion coefficient. The mesh size becomes smaller and the corresponding diffusion faster as the cross-linking proceeds, and consequently the relaxation time is decreased again. The mentioned divergence is, of course, experimentally not directly observable. This picture is in full agreement with de Gennes' treatment for ideal networks.

Another criterion for the gel point was considered by Martin and Wilcoxon[50] who noticed in their studies on

silica gels that the field time correlation function at the gelpoint follows a power law behavior with an exponent between $n = 0.5$ and 0.67. Such power law behavior was also observed with our system in the temperature range from 42 to 48 °C. The exponents at the temperatures 42, 45, and 48 °C were $n = 0.64$, 0.63, and 0.51, respectively with an error ±0.01. A gradual decrease of the exponent was also observed by Norisuye et al.[16] when moving away from the gel point toward the gel state. Below 42 °C and above 48 °C, the behavior of stretched exponential was obtained. Thus, the gel point can be estimated to lie between 42 and 45 °C which is in good agreement with the maximum of the fast relaxation time shown in Figure 13. According to Muthukumar[51] and Martin et al.[52] the exponent n is related to the fractal dimension d_f of the structures in the gel as follows

$$n = \frac{3(5 - 2d_f)}{2(3 - d_f)} \tag{26a}$$

or

$$d_f = \frac{7.5 - 3n}{3 - n} \tag{26b}$$

which with $n = 0.63 \pm 0.01$ gives $d_f = 2.37 \pm 0.06$ a value that is characteristic of branched structures a conclusion that was drawn already previously in this paper.

If heterogeneities are formed with a higher than average segment density (formed for instance via association) and these are not frozen-in, then an additional slow motion occurs, that further will increase as cross-linking proceeds. Such behavior is found with the present system and that of Norisuye et al.[16] and was also observed by Fuchs et al.[10,11] with a thermally reversible gel and by Coviello et al.[13] for an ion-induced physical gel.

Now, depending on the treatment, the slow relaxation processes (Figure 14) appear to occur on very different time scales, but the overall trends are similar. This quantitative disagreement of $\langle\tau\rangle_2$ was expected because the two experiments covered different time scales. The data collected in one spatial orientation ($g_T(q,\tau)$) and treated with the heterodyne approach extended to 10^6 μs, whereas the data collected over all spatial orientations ($g_E(q,\tau)$) extends only to 10^4 μs. For the nonergodic approach all relaxation process with $\langle\tau\rangle_2 > 10^4$ μs, are considered as essentially frozen-in. For the heterodyne approach, on the other hand, only all relaxation processes with $\langle\tau\rangle_2 > 10^6$ μs are assumed being of static origin, and processes with relaxation times of $10^4 > \langle\tau\rangle_2 > 10^6$ μs are included. The difference in the relaxation times is thus just an experimental artifact that is not taken into consideration in the difference between the two approaches. Actually the assumption of fully frozen-in components is too strong a simplification for realistic systems. Pusey and van Megen[4] estimated when nonergodic behavior has to be expected and when not. The boundary between the two behaviors was given by the quantity $q\delta > 1$ (ergodic) and $q\delta < 1$ (nonergodic), where δ is the amplitude of fluctuation around fixed average positions.[18] Slowly migrating heterogeneities as were considered by Bastide et al.[15] and theoretically treated by Panyukov and Rabin[14] were not taken into account.

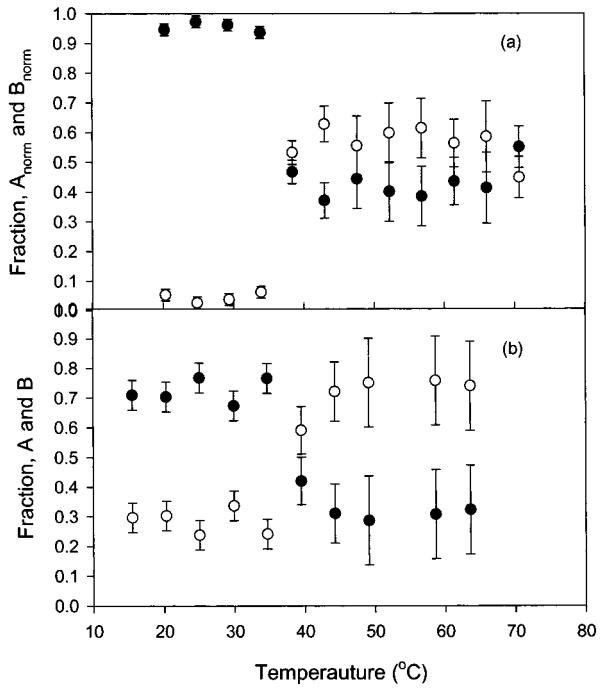

Figure 15. (a) $A_{norm} = A/C$ and $B_{norm} = B/C$ for the nonergodic analysis. (b) A and B for the heterodyne approach.

The relaxation times presented in Figure 14 are mean relaxation times calculated from eqs 22 and 25. In a previous paper by Fuchs et al.,[10] the stretch exponent, β, was found to decrease for both the fast and slow modes over the gelation process. No similar trend was observed for either the nonergodic or heterodyne analysis with β remaining constant within experimental error for both the fast and slow processes. The difference in behavior may result from the fact that Fuchs et al.[10] studied a thermoreversible gel, whereas the present system and that of Joosten et al.[17] are permanent gels. This again shows that the oversimplification of frozen-in components may lead to unexpected properties.

The relative contributions of the fast and the slow processes may be considered by plotting A and B respectively from eq 25 for the heterodyne and the nonergodic treatment where $A_{norm} = A/C$ and $B_{norm} = B/C$. The results are show in Figure 15. In both cases, the fast mode dominates the solution behavior. After the gel transition, the slow mode (B and B_{norm}) clearly dominates the behavior for the heterodyne approach, whereas for the nonergodic approach the slow mode (B_{norm}) is less dominant. Because of the longer time scale of measurements the heterodyne approach includes more of the slower processes than the nonergodic approach.

Angular Dependence in the Gel and Liquid States: the Nonergodic Approach. The nature of the gel and the liquid states can be investigated further by consideration of the diffusive properties as a function of q. The angular dependence of the relative contributions of the fast and slow components is shown in Figure 16. It should be noted that B_{norm} before gelation is very small (0.05 ± 0.02) suggesting an almost negligible contribution of a slow motion in the solution state. This is in agreement with the results obtained for xanthan in the absence of cross-linker. The exponential stretches for both modes (β_1 and β_2) fits were found to be independent of q^2. Surprisingly the amplitude factors show no angular dependence in the gel and the liquid

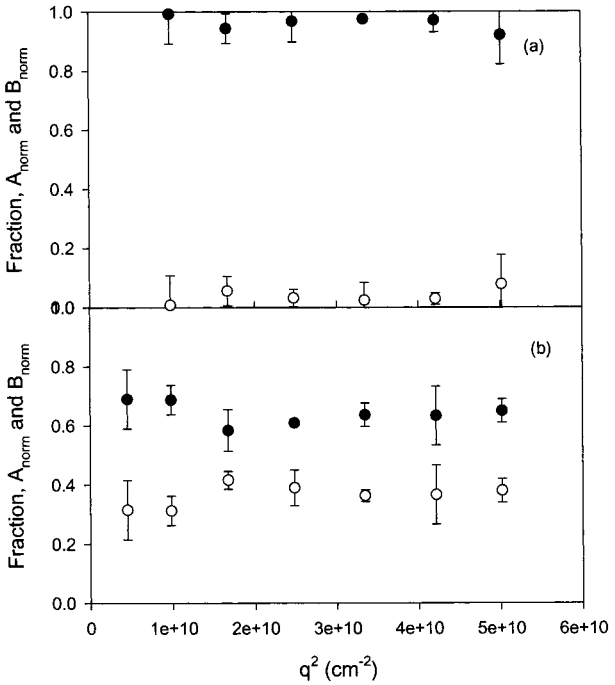

Figure 16. Angular dependence of $A_{norm} = A/C$ (closed circles)- and $B_{norm} = B/C$ (open circles) for the nonergodic analysis eq 30: (a) measured at $T = 15$ °C, giving $C = 0.05 \pm 0.02$; (b) measured at $T = 72$ °C, giving $C = 0.90 \pm 0.05$.

states. This indicates a slow motion that is not affected by the size of the heterogeneities but rather by the local viscosity, since large clusters have a strong angular dependence.

Finally the angular dependence of the reciprocal relaxation times shall be discussed. The values of $\langle\tau\rangle^{-1}q^{-2}$ gives an apparent diffusion coefficient, $D_{app}(q)$, that for flexible objects often depends on the scattering angle. Parts a and b of Figure 17 show the results for the fast and slow apparent diffusion coefficients, respectively. Very different behavior is found for the fast and slow motions in the solution state (at 15 °C) and the gel state (72 °C).

In *solution* the apparent diffusion coefficients show linear increase with q^2. Such behavior was previously predicted[53] for partially flexible objects to follow the relationship:

$$D_{appg}(q) = D_c\,(1 + CR_g{}^2q^2 - ...) = D_c(1 + C'R_h{}^2q^2 - ...) \quad (27)$$

where the dimensionless parameters C and C' depend on the slowest relaxation time in a particle. The predicted values range from $C = 0.20$ for flexible linear chains to $C = 0.10$ for densely branched flexible chains down to $C = 0$ for hard spheres and is thus a measure of the internal flexibility. Unfortunately the radii of gyration were not measured, but the hydrodynamic radii could be calculated from the diffusion coefficients which gave $R_{h,fast} = 147$ nm and $R_{h,slow} = 5670$ nm resulting in values for $C'_{fast} = 0.076$ and $C'_{slow} = 0.117$. If we assume behavior of branched objects consistently, we find $C_{fast} = C_{slow} = 0.100 \pm 0.018$ in agreement with our assumption of a rather flexible branched structure.

In the *gel state* (72 °C) the apparent diffusion coefficients *decrease* with q^2. Such behavior is to be expected. If a dominant internal relaxation is superimposed to the translational motion of the collective

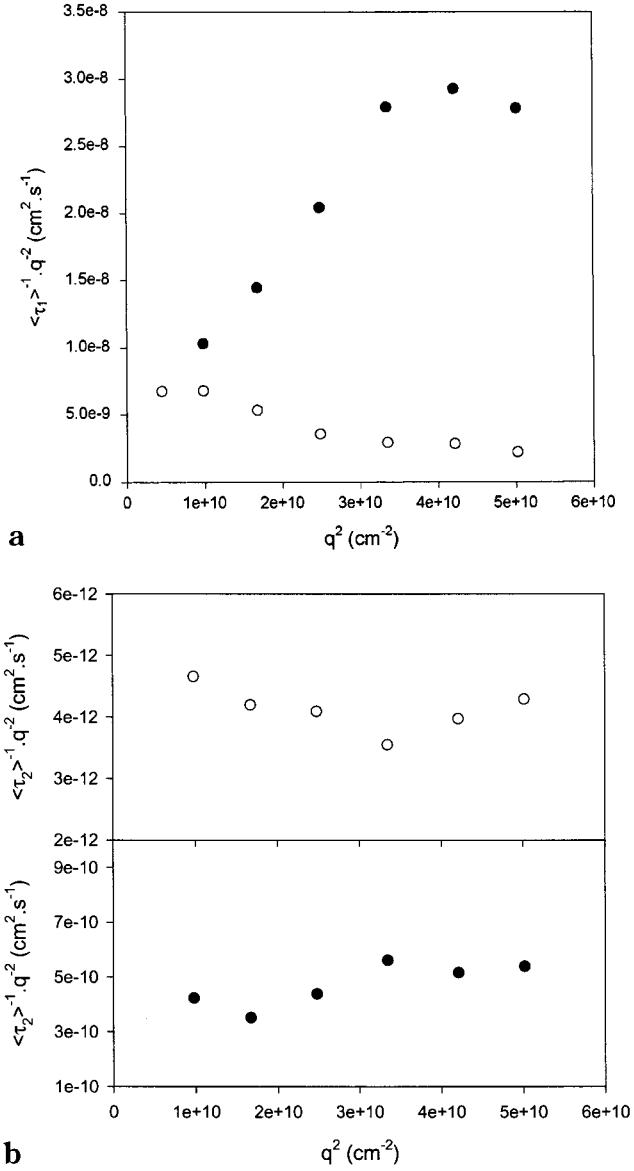

Figure 17. Angular dependence of $D_{app} = \langle\tau_1\rangle^{-1}q^{-2}$ for both modes. (a) Fast mode denoted subscript 1, $T = 15$ °C (closed) and $T = 72$ °C (open). (b) Slow mode denoted subscript 2, $T = 15$ °C (closed) and $T = 72$ °C (open). The linear increase of the apparent diffusion coefficient for the two types of motion in the solution gives indications to internal flexibility of the macromolecular objects (see eq 26). The downward curvature for the two motions in the gel state indicated the presence of a pronounced contribution of internal motions that is further evaluated in Figure 18.

diffusion. Theory[12] predicts in such a case that the average reciprocal relaxation time is given by a sum of two components as

$$\left\langle\frac{1}{\tau}\right\rangle = \frac{1}{\tau_{int}} + D_{app}\,(q)q^2 \quad (28)$$

where the subscript *int* means internal motion, and the angle bracket indicates the average over a relaxation spectrum. Figure 18 shows the plot of $\langle 1/\tau_{fast}\rangle$ and $\langle 1/\tau_{slow}\rangle$ against q^2 for the sample at 72 °C, deep in the gel state. In both cases, a finite intercept is obtained which correspond to relaxation times of $\tau_{int,fast.} = 0.022$ s and $\tau_{int,slow.} = 36.7$ s. We are not able to decide whether these relaxations correspond to orientational fluctuation of a stiff director or whether it has to be assigned to something like a breathing mode of the network.

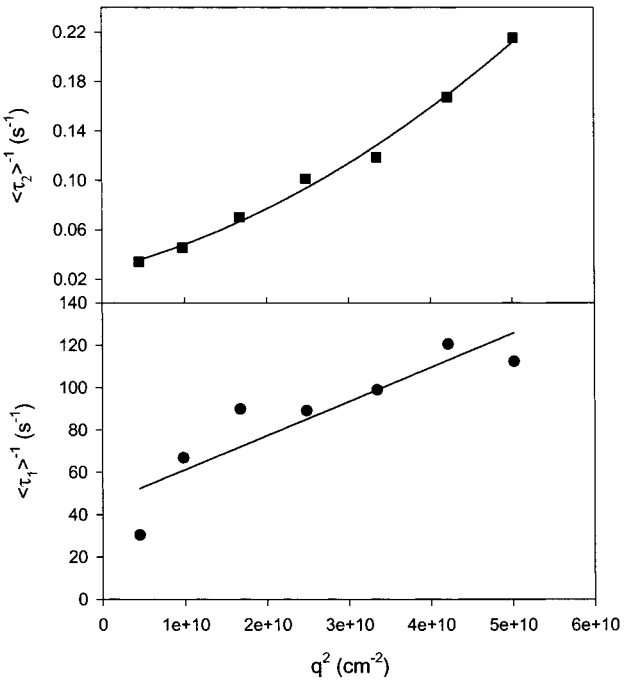

Figure 18. Pot plot of the average reciprocal modes of motion in the gel as a function of q^2 (see eq 27). Subscripts 1 and 2 denote fast and slow modes, respectively. The intercept is related to a purely internal motion (without translational motion) and the initial slope gives the value for the collective diffusion of the two in the gel. The slight curvature in the plot for the slow motion indicated the additional effect of internal mobility that is superimposed to the translational diffusion. Squares represent the slow relaxation times, and circles represent the fast relaxation times.

Table 1. Analysis Data from Static and Dynamic Light Scattering for Xanthan with and without Heat Treatment[a]

	xanthan in 5000 ppm NaCl	
	without heat treatment	with heat treatment
R_g (nm)	409	315
M_w (g/mol)	1410×10^6	78×10^6
A_2 (mol/mL/g^2)	1.03×10^{-5}	4.59×10^{-5}
$c^* = 1/(M_w A_2)$ (mg/mL)	0.06	0.24
D_{trans} (cm^2/s)	3.15×10^{-9}	
R_h (nm)	909	
ρ ($=R_g/R_h$)	0.45	

[a] All measurements made at $T = 20$ °C.

Table 2. Analysis Data from the Angular Dependencies of the Fast and Slow Motions in the Solution (15 °C, before Gelation) and the Gel State (72 °C)

	15 °C	72 °C
D_{fast} (cm^2/s)	1.21×10^{-9}	1.03×10^{-9}
$R_{h,fast}$ (μm)	0.147	0.682
C_{fast}	0.076	
D_{slow} (cm^2/s)	3.15×10^{-10}	2.16×10^{-12}
$R_{h,slow}$ (μm)	5.67	325
C_{slow}	0.117	
$\tau_{int,fast}$ (s)		0.02
$\tau_{int,slow}$ (s)		36.76

The limiting slopes at $q = 0$ of the curves in Figure 18 give the apparent diffusion coefficient of the two translational collective diffusion coefficient. The values are given in Table 2. We have already seen that the fast motion can be assigned to the mesh size of the network, but a quantitative estimation cannot be made, because of a pronounced increase in the local viscosity. The origin of the slow motion is not as clear and may result from clusters formed already in the solution state, but the motion is now immensely reduced after gelation, again by an increase in the friction, due to the constraints of the network. The factors of reduction in the diffusion coefficients are 1.2 and 145 for the fast and slow motion. There may be a further increase in the heterogeneity domain, but additional measurements are required, (e.g., detailed static light and small-angle neutron scattering) if we wish to differentiate between the effects of increased local viscosity or the radius of gyration. In the present experiment, we only can measure the frictional coefficient after applying the Einstein relationship, given as $f_c = 6\pi\eta(c)R_h(c)$. These very slow motions do not cause the nonergodic behavior of frozen-in components. These processes are even much longer.

Conclusion

The main problem of dynamic light scattering is the occurrence of a nonergodic or pseudo nonergodic behavior. The two derived approaches, (heterodyne and nonergodic treatments) start with essentially the same assumption of frozen-in heterogeneities. The two approaches differ, however, significantly in the normalization. In the heterodyne approach only one position is chosen and the intensity TCF is normalized by the *time average* asymptote whereas in the nonergodic approach the normalization is made with regard of the *ensemble average*. In the presence of nonmoving scattering objects, which are more or less randomly distributed in space, significant differences are observed depending on whether in the heterodyne experiment just a large speckle is recorded or not. In this case the nonergodic approach, which includes an additional ensemble average, is the more accurate one. However, if a sufficiently large number of such speckles is in the scattering volume, the obtained results from the nonergodic treatment are comparable with those from the heterodyne treatment. The heterodyne contribution $(1 - X)$ was found in these cases to be very similar in value to the asymptotic plateau height in the field TCF of the nonergodic approach.

Often, however, measurement of the TCF at different positions gave the same result, if the recording time was chosen long enough. Such case is obtained when the heterogeneities are not fully frozen-in but still possess a very slow mobility,[13,48] for instance in physical networks where association and dissociation can take place. For practical reasons, such long recording times cannot be applied when using common autocorrelators, and the nonergodic approach with much shorter recording times has to be used. In this case, one has to be aware that on a long scale the apparent frozen heterogeneities may actually be slightly mobile and will be responsible for aging effects over the course of several days.[48] The present system belongs partly to the last example. Evidently there is a frozen component present, but the nonergodic approach added slowly moving heterogeneities to the immobile moiety and overestimates the really immobile fraction.

The *fast* motion was found in both approaches to be almost identical. The relaxation time as a function of temperature shows typical behavior of a gelling system with a divergence at the gel point. This temperature agrees with the temperature for the onset of heterodyne or nonergodic behavior. Thus, a gel point can be found

also by dynamic light scattering by observation of these two quantities. In the solution state, the fast motion clearly results from the translational motion of the particles that grow as a result of cross-linking, and after the gel point, it is related to the mesh size of the network. No quantitative estimation of the actual size can be made, because of an increase of the local viscosity in the network. Both of these motions contain influences from internal flexibility.

At this point we wish to stress that it is the relaxation time that represents the relevant quantity to consider rather than an apparent diffusion coefficient, whose determination depends on the technique to which extent the frozen component is taken into account. The relaxation times from the heterodyne and nonergodic experiments agree within experimental error, but the apparent diffusion coefficients can be very different, as was already outlined by Joosten et al.[17]

The origin of the *slow* motion *in the network* remains for the same reason ambiguous. The heterogeneity may have increased, but certainly not by a factor of 156 that would give a hydrodynamic radius of 0.3 mm (!). The results can likewise be explained by the corresponding increase of the local viscosity. Interestingly, these *fast and slow* motions are not fully translational but contain an appreciable contribution from purely internal modes of motion. These could arise from orientational or breathing modes of the network.

Acknowledgment. The work was kindly supported by the German Academic Exchange Program (DAAD). It is partly funded by a special Investigators Grant from the Australian Research Council awarded to D.V.B and the Particulate Fluids Processing Centre at the University of Melbourne. A.B.R. would like to gratefully acknowledge the support and assistance of the Freiburg research group of Professor Walter Richtering, now at the University of Kiel, Germany.

References and Notes

(1) Nolte, H.; John, S.; Smidsrod, O.; Stokke, B. T. *Carbohydr. Polym.* **1995**, *18*, 243.
(2) Shu, P. *ACS Symp. Ser.* **1989**, *396*, 137.
(3) Rodd, A. B.; Cooper-White, J.; Dunstan, D.; Boger, D. V. *Polymer* **2000**, *Submitted*.
(4) Pusey, P. N.; van Megen, W. *Physica A* **1998**, *157*, 705.
(5) Geissler, E. In *Dynamic Light Scattering from Polymer Gels*; Brown, W., Ed.; Clarendon Press: Oxford, England, 1993; Chapter 11.
(6) Horkay, F.; Geissler, E.; Hecht, A.; Zrinyi, M. *Macromolecules* **1989**, *21*, 2589.
(7) Tanaka, T.; Hocker, L. O.; Benedek, G. B. *J. Chem. Phys.* **1973**, *59*, 5151.
(8) Munch, J. P.; Candau, S. J.; Hertz, J.; Hild, G. *J. Phys. (Paris)* **1977**, *1977*, 911.
(9) Hecht, A.; Guillermo, A.; Horkay, F.; Mallam, S.; Legrand, J. F.; Geissler, E. *Macromolecules* **1992**, *25*, 3677.
(10) Fuchs, T.; Richtering, W.; Burchard, W.; Kajiwara, K.; Kitamura, S. *Polym. Gels Networks* **1997**, *5*, 541.
(11) Richtering, W.; Fuchs, T.; Burchard, W. *Ber. Bunsen-Ges. Phys. Chem.* **1998**, *102*, 1660.
(12) Berne, B. J.; Pecora, R. *Dynamic Light Scattering:* Wiley: New York, 1976.
(13) Coviello, T.; Burchard, W.; Geissler, E.; Maier, D. *Macromolecules* **1997**, *30*, 2008.
(14) Panyukov, S.; Rabin, Y. *Macromolecules* **1996**, *29*, 7960.
(15) (a) Bastide, J.; Leibler, L.; Prost, J. *Macromolecules* **1990**, *23*, 1821. (b) Rouf, C.; Bastide, J.; Pujol, J. M.; Schossler, F.; Munch, J. P. *Phys. Rev. Lett.* **1994**, *73*, 830.
(16) Norisuye, T.; Inoue, M.; Shibayama, M. Tamaki, R.; Chujo, Y. *Macromolecules* **2000**, *33*, 900.
(17) Joosten, J. G. H.; McCarthy, J. L.; Pusey, P. N. *Macromolecules* **1991**, *24*, 6690.
(18) Shibayama, M. *Macromol. Chem. Phys.* **1998**, *199*, 1.
(19) (a) Flory, P. J. *Principles of Polymer Chemistry*; Cornell University Press: Ithaca, NY, 1953. (b) Flory, P. J. *J. Am. Chem. Soc.* **1941**, *63*, 3083, 3091, 3096.
(20) Stockmayer, W. H. *J. Chem. Phys.* **1943**, *11*, 45; **1944**, *12*, 105.
(21) Stauffer, D. *Introduction to Percolation Theory*; Taylor and Francis: London, 1985.
(22) de Gennes, P. G. *Scaling Concepts in Polymer Solutions*; Cornell University Press: London, 1979.
(23) Pusey, P. J. *Macromol. Symp.* **1994**, *79*, 10.
(24) Siegert, A. J. F. *MIT Rad. Lab. Rep.* **1944**, 465.
(25) Zimm, B. H. *J. Chem. Phys.* **1948**, *16*, 1099.
(26) Burchard, W. Light Scattering Techniques In *Physical Techniques for Study of Food Biopolymers*; Ross-Murphy, S. B., Ed.; Blackie Academic & Professional: London, 1995, Chapter 4.
(27) Berry, G. C. *J. Chem. Phys.* **1966**, *44*, 4550.
(28) (a) Guinier, A. *Ann. Phys.* **1939**, *12*, 161. (b) Guinier, A.; Fournet, G. *Small Angle Scattering of X-rays*; Wiley: New York, 1955.
(29) See, for instance: Huglin, M. B. *Light Scattering from Polymer Solutions*; Academic Press: London, 1972.
(30) Morris, V. J.; Frankline, D.; I'Anson, K. *Carbohydr. Res.* **1983**, *18*, 131.
(31) Milas, M.; Rinaudo, M. *Carbohydr. Res.* **1979**, *76*, 189.
(32) Ross-Murphy, S. B.; Morris, V. J.; Morris, E. R. *Faraday Symp. Chem. Soc.* **1983**, *18*, 115.
(33) Dentini, M.; Coviello, T.; Kajiwara, K.; Crescenzi, V.; Burchard, W. *Macromolecules* **1982**, *21*, 3312.
(34) Berth, G.; Dautzenburg, H.; Christensen, B. E.; Harding, S. E.; Rother, G.; Smidsrod, O. *Macromolecules* **1996**, *29*, 3491.
(35) Holzwarth, G. *Carbohydr. Res.* **1978**, *66*, 173.
(36) Capron, I.; Brigand, G.; Muller, G. *Polymer* **1997**, *38*, 5289.
(37) Casassa, E. F. *J. Chem. Phys.* **1955**, *23*, 596.
(38) Holtzer, A. *J. Polym. Sci.* **1955**, *17*, 432.
(39) (a) Sato, T.; Norisuye, T.; Fujita, H. *Macromolecules* **1984**, *17*, 2696. (b) Sato, T.; Norisuye, T.; Fujita, H. *Polymer* **1984**, *16*, 341.
(40) Kratky, O.; Porod, G. *J. Colloid Sci.* **1949**, *4*, 35. Burchard, W. *Macromolecules* **1974**, *7*, 841.
(41) (a) Burchard, W. *Macromolecules* **1974**, *7*, 841; (b) *Macromolecules* **1977**, *10*, 919; (c) *Adv. Polym. Sci.* **1983**, *48*, 1.
(42) Denkinger, P. Burchard, W. *J. Polym. Sci.; Phys. Ed.* **1991**, *29*, 589.
(43) Vogel, H. J.; Burchard, W. *Comput. Theor. Polym. Sci.* **2000**, *10*, 133.
(44) (a) Williams, G.; Watts, D. C. *Trans. Faraday Soc.* **1970**, *66*, 80. (b) Williams, G.; Watts, D. C.; Worth, A. M. *Trans. Faraday Soc.* **1971**, *67* 1323.
(45) Kohlrausch, R. (a) *Poggendorff Anal. Chem.* **1854**, *91*, 179; (b) **1863**, *119*, 337.
(46) Burchard, W.; Schmidt, M.; Stockmayer, W. H. *Macromolecules* **1980**, *13*, 1265.
(47) Schmidt, M.; Nerger, D.; Burchard, W. *Polymer* **1979**, *20*, 582.
(48) Cipelletti, L-; Manley, S.; Ball, R. C.; Weitz, D. A. *Phys. Rev. Lett.* **2000**, *84*, 2275.
(49) Burchard, W.; Lang, P.; Schulz, L.; Coviello, T. *Makromol. Chem., Macromol. Symp.* **1992**, *58*, 21.
(50) Martin, J. E.; Wilcoxon, J. *Phys. Rev. Lett.* **1988**, *61*, 373.
(51) (a) Muthukumar, M. *J. Chem. Phys.* **1985**, *83*, 367; (b) *Macromolecules* **1989**, *22*, 4656.
(52) Martin, J. E.; Adolf, D.; Wilcolxon, P. *Phys. Rev. Lett A* **1989**, *39*, 1325.
(53) Burchard, W.; Schmidt, M.; Stockmayer, W. H. *Macromolecules* **1980**, *13*, 580.

MA001706G